Research Article Vol. 28, No. 1 / 6 January 2020 / Optics Express 485
Optics EXPRESS

Tunable strong coupling of two adjacent optical $\lambda/2$ Fabry-Pérot microresonators

ACHIM JUNGINGER,[1] FRANK WACKENHUT,[1,4] ALEXANDER STUHL,[1,2] FELIX BLENDINGER,[3] MARC BRECHT,[1,2] AND ALFRED J. MEIXNER[1,5]

[1] *Institute of Physical and Theoretical Chemistry, Eberhard Karls University, 72076 Tübingen, Germany*
[2] *Process Analysis and Technology, Reutlingen University, 72762 Reutlingen, Germany*
[3] *Faculty for Mechanical and Medical Engineering, Furtwangen University, 78054 Villingen-Schwenningen, Germany*
[4] *frank.wackenhut@uni-tuebingen.de*
[5] *alfred.meixner@uni-tuebingen.de*

Abstract: Strong optical mode coupling between two adjacent $\lambda/2$ Fabry-Pérot microresonators consisting of three parallel silver mirrors is investigated experimentally and theoretically as a function of their detuning and coupling strength. Mode coupling can be precisely controlled by tuning the mirror spacing of one resonator with respect to the other by piezoelectric actuators. Mode splitting, anti-crossing and asymmetric modal damping are observed and theoretically discussed for the symmetric and antisymmetric supermodes of the coupled system. The spectral profile of the supermodes is obtained from the Fourier transform of the numerically calculated time evolution of the individual resonator modes, taking into account their resonance frequencies, damping and coupling constants, and is in excellent agreement with the experiments. Our microresonator design has potential applications for energy transfer between spatially separated quantum systems in micro optoelectronics and for the emerging field of polaritonic chemistry.

Optical $\lambda/2$ microresonators are structures that confine light to volumes with dimensions on the order of half a wavelength and enable to control and study light-matter interaction. The interaction between a quantum system and an optical field confined in a microresonator can be divided into the weak and strong coupling regime. In the weak coupling regime, the respective decay rates are larger than the coupling rate between the quantum system and the microresonator. In this case, the spontaneous emission of the quantum system is altered with respect to the free space, a phenomenon known as Purcell effect [1–6]. To reach the strong coupling regime, the coupling strength between the optical field in the resonator and the quantum system must be considerably larger than their respective decay rates. This leads to new hybrid polaritonic states [7], which have an energy difference proportional to the coupling strength. The spectral signature is a splitting of the transmission spectrum into two polaritonic modes, referred to as Rabi splitting [8]. When the cavity resonance is tuned over the eigenfrequency of the quantum system, anticrossing is observed in the dispersive behavior of the polaritonic modes [9]. The first observation of strong coupling between electromagnetic fields and a quantum system has been shown by the interaction between Rydberg atoms and a high Q microwave resonator at cryogenic temperatures [10]. Since then, different optical experiments showing strong light matter coupling have been accomplished using metal or dielectric resonators [9,11–18], photonic crystals [19,20], micropillars [21], coated fibers [22] or microdisks [23]. Today, strong coupling has been shown for ensembles down to single molecules that couple to cavity fields, as well as to plasmonic modes [24–30]. Recently, strong coupling has been used to influence chemical reactions, e.g. by strong coupling of molecular vibrations to an infrared resonator by altering the chemical reaction rate involving this particular vibration [31–33].

#380068 https://doi.org/10.1364/OE.380068
Journal © 2020 Received 9 Oct 2019; revised 5 Dec 2019; accepted 11 Dec 2019; published 2 Jan 2020

Optics EXPRESS

Another important area is strong coupling of purely optical modes, which has been extensively studied in various systems, e.g. phase-locked semiconductor laser arrays [34], coupled optical or photonic fibers [35–38]. More recently, strong coupling of optical modes has gained increasing attraction in microstructures such as photonic molecules [39–43] or photonic crystal cavities [44–46], which can even show lasing [44]. The superposition of strongly coupled optical modes leads to frequency splitting and the formation of supermodes, which can have symmetric or antisymmetric parity and different losses [47].

Here, we will study the pure optical mode-coupling between two microresonators consisting of three silver mirrors with a minimal mirror spacing of half a wavelength, suitable for resonances in the visible spectral region. This is, to the best of our knowledge, the first report on direct optical mode coupling between two $\lambda/2$ Fabry-Pérot resonators. We show that such a coupled microresonator can have remarkable large coupling constants, which enables to observe strong coupling despite the low Q factor (~70-100) of the individual resonators. An advantage of such a microresonator is, that it can be easily fabricated by evaporating layers of different reflectivities and allows to have full control over all parameters, i.e. resonance frequency, damping and coupling constant. Additionally, the resonance frequency can be precisely tuned (~5 nm) over several free spectral ranges. Therefore, such a microresonator is an ideal model system to study strong coupling effects since the coupling strength can be tailored by changing the properties of the central mirror and the tuneability of the mirror spacing over a wide range. Additionally, the combination of light matter and pure optical mode coupling could lead to interesting new applications, such as coupling of quantum systems over large spatial distances with efficient energy transfer or in polaritonic chemistry.

As a reference, we consider a single microresonator (Fig. 1(a)) consisting of two silver mirrors separated by half a wavelength in the visible spectral region [48]. The resonance of the microresonator can be precisely tuned by changing the mirror separation z with piezo actuators in steps of down to 5 nm. The mirrors are fabricated from microscopy cover slides by electron beam evaporation of a 50 nm thick silver layer, followed by a 10 nm gold layer and a protection layer of 10 nm $Si0_2$. The final resonator structure is assembled in a home-built holder with piezo actuators (KC1-PZ/M, Thorlabs) and immersion oil between the two mirrors. The coupled resonator is schematically shown in Fig. 1(b). The top mirror is identical to the single microresonator, but the lower mirror is replaced by a microresonator with a fixed optical path length. It consists of a 50 nm thick silver layer on top of the lower cover slip followed by a transparent $Si0_2$ spacer layer of 145 nm thickness which is covered with a silver layer of variable thickness and is shared by both resonators. Additionally, a 10 nm thick gold and a 10 nm $Si0_2$ layer are used to protect the central mirror against the immersion oil in the upper resonator. The central silver layer has a thickness of 14 nm, 24 nm or 38 nm giving reflectivities of 66%, 85% and 95%, respectively, resulting in different coupling constants κ between the upper and lower resonator. Transmission spectra are recorded by illuminating the microresonator through the upper mirror with a white light LED operating under continuous wave conditions. The transmitted light is collected from below with a home built confocal microscope equipped with an oil immersion objective lens (NA = 1.46) and a spectrometer with a CCD-detector. Figures 1(c) and 1(d) show the respective experimental (blue line) and simulated (green dashed line) transmission spectra of the single and coupled microresonator, respectively. For a single microresonator only one Lorentzian shaped transmission peak is observed, while the coupled system shows two transmission peaks separated by the Rabi splitting $\Delta\Omega$. Deviations from the Lorentzian line shape at higher energies occur due to off-axis modes, which are detected due to the high NA of the objective lens [49].

Since the transmission spectrum of a single resonator can be fitted for stationary conditions by a Lorentzian line shape function we may describe the autocorrelation function of the transmitted

Optics EXPRESS

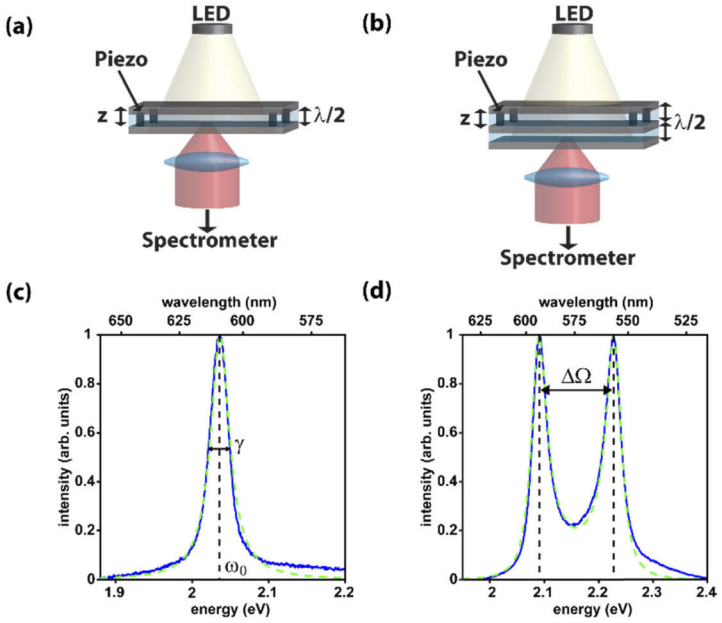

Fig. 1. (a) Schematic drawing of a single tunable microresonator consisting of two parallel silver mirrors. (b) Schematic drawing of two coupled microresonators, which are separated by a partially transmitting silver mirror where the lower resonator is fixed and the upper resonator can be tuned. The resonators are illuminated with a white light LED from the top. Piezo actuators allow to tune the optical path length z with high precision within the $\lambda/2$ region of the visible spectral range. (c) Transmission spectrum (blue line) of the single microresonator, which is fitted by a Lorentzian line shape (green dashed line) of a harmonic oscillator. (d) Transmission spectrum of the coupled microresonators (blue line) with two transmission maxima fitted by the spectral line shape (green dashed line) of two coupled harmonic oscillators that have identical eigenfrequencies ω_0, separated by the Rabi splitting $\Delta\Omega$.

signal by a damped harmonic oscillator with an amplitude given by:

$$x(t) = \exp\left(-\frac{\gamma t}{2}\right)[\cos(\omega_d t)]\ ,\ \omega_d = \sqrt{\omega^2 - \left(\frac{\gamma}{2}\right)^2} \tag{1}$$

with the resonance frequency ω_d and the damping constant γ. Figure 2(a) displays the analytical solution x(t) in red and the Fourier transform of the time dependent amplitude x(t) is shown by the red dashed line in Fig. 2(b). The blue lines in Figs. 2(a) and 2(b) are the respective numerical solutions for a single damped harmonic oscillator. The inset in Fig. 2(a) presents the first 2.5 periods and shows the good agreement between the analytical and numerical solution. This approach gives a Lorentzian line shape, which is in perfect agreement with the experimental data shown in Fig. 1(c). In the following, we model the autocorrelation function of the coupled system by two coupled damped harmonic oscillators for which the respective power spectral density can be calculated by Fourier transformation. The equations of motion for the amplitudes of the two coupled harmonic oscillators are described by two coupled differential equations, which can be written as:

$$\begin{aligned} \ddot{x}_1(t) + \gamma_1 \dot{x}_1(t) + \omega_1^2 x_1(t) + \kappa x_2(t) = 0 \\ \ddot{x}_2(t) + \gamma_2 \dot{x}_2(t) + \omega_2^2 x_2(t) + \kappa x_1(t) = 0 \end{aligned} \tag{2}$$

Optics EXPRESS

with the damping constants γ_1, γ_2 and the resonance frequencies ω_1, ω_2 of the two individual oscillators and the respective coupling constant κ. The damping constants were determined from the experimental transmission spectra for large detuning of the resonators and were kept constant during the calculations. This assumption is justified due to the weak dispersion of the used materials in the spectral region investigated in this work [50].

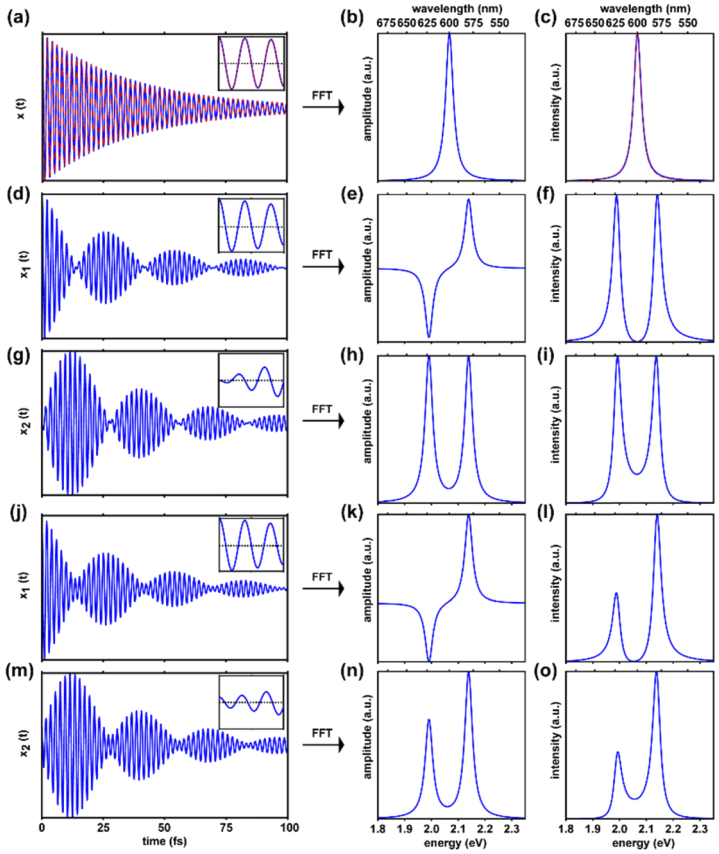

Fig. 2. (a) Analytical (red, Eq. (1)) and numerically calculated (blue) decay of the amplitude x(t) of a damped harmonic oscillator. The insets show the first 2.5 periods of the oscillation. The amplitude (b) and the absolute square (c), i.e. the spectrum, of the Fourier transform of x(t) shown in (a) has a single peak at ω (expressed in eV). The red curve is a Lorentzian shaped analytical solution and validates the procedure. (d) and (g) illustrate the temporal response of two coupled oscillators with the same resonance frequency and damping constant, where the second oscillator is exclusively excited by coupling to the first one ($x_1(0) = 1$, $x_2(0) = 0$, see inset in (d) and (g)). A beating pattern can be observed due to the energy exchange between the oscillators. The amplitudes (e) and (h) and the absolute square (f) and (i) of the corresponding Fourier transforms exhibit two maxima caused by strong coupling. These modes are the antisymmetric (e)/symmetric (h) supermodes of this coupled system. In (j) and (m) all parameters are the same as in (d) and (g), but the starting condition of the second oscillator was set to $x_2(0) = 0.2$, which can be seen in the inset in (m). This change induces an intensity difference in the spectral response of the coupled system.

By solving these equations numerically, we obtain $x_1(t)$ and $x_2(t)$, which are supermodes of the coupled system and are shown in Figs. 2(d) and 2(g), respectively. The coupled system is illuminated from the top and therefore we set the starting amplitude of the first oscillator

Optics EXPRESS

to $x_1(0) = 1$, while it is zero for the second one $x_2(0) = 0$, which can be seen in the inset in Figs. 2(d) and 2(g). In this case the second oscillator $x_2(t)$ is exclusively excited via the coupling to $x_1(t)$. After the excitation of $x_1(t)$ the energy is transferred to $x_2(t)$ and since the transfer is allowed in both directions the energy is transferred back to $x_1(t)$. Due to this coherent energy exchange we can observe a beating pattern in the temporal response $x_{1/2}(t)$. Again, the power spectral density of the coupled resonators is proportional to the Fourier transforms of $x_{1/2}(t)$. The amplitudes of the Fourier transform are presented in Figs. 2(e) and 2(h) for the special case of $\omega_1 = \omega_2$. The absolute square of the Fourier transform is shown in Figs. 2(f) and 2(i), which are the antisymmetric (Figs. 2(e) and 2(f)) and symmetric (Figs. 2(h) and 2(i)) supermodes of the coupled system. The calculated spectra show two resonator modes, which are spectrally separated by the Rabi splitting $\Delta\Omega$. Figures 2(j) and 2(m) illustrate the case when $x_2(t)$ is not exclusively excited by coupling to $x_1(t)$, but is in addition directly excited by a small amount due to finite reflectivity of the upper two mirrors. We include this in our simulations via the starting conditions by setting $x_1(0) = 1$ and $x_2(0) = 0.2$, as shown in the inset of Figs. 2(j) and 2(m). This change in the starting condition leads to an intensity difference between the two spectral peaks observed in the spectra in Fig. 2(l) and 2(o). These results are in good agreement with FDTD calculations e.g. by Atlasov *et al.* [47].

We can fit this equation to the experimental transmission spectra shown in Figs. 1(c) and 1(d) and find a perfect agreement for both the single and coupled system. An exemplary spectrum of the coupled microresonator is shown in blue in Fig. 1(d) together with a simulation based on two coupled harmonic oscillators with $\lambda_1 = \lambda_2 = 573.4$ nm, $\gamma_1 = \gamma_2 = 34.5$ meV and κ=0.465 eV. By comparing the experimental spectrum to $x_1(\omega)$ and $x_2(\omega)$ we find a perfect agreement with $x_2(\omega)$, which can be explained since we detect from below and only light fulfilling the resonance condition of the coupled microresonators can reach the detector.

In order to prove that the splitting observed in Fig. 1(d) is caused by strong coupling we have investigated the dispersion of the microresonator modes. This can be achieved by tuning the resonance of the upper resonator across the resonance of the lower one. The results of this experiment are illustrated in Fig. 3. For comparison, Fig. 3(a) shows experimental data for a single microresonator where the resonance is tuned from 505 nm to 611 nm. The intensity modulation seen in the experimental spectra is caused by the emission profile of the white light LED and is also considered in the simulations. Figure 3(b) displays the corresponding simulation of the single microresonator where the resonances are adjusted to match the experimental data shown in Fig. 3(a). We find a perfect agreement between the simulated and experimental dispersion, which shows that harmonic oscillators can be utilized to model such microresonator systems. Figure 3(c) presents a schematic representation of the resonator geometry where the resonance of the upper resonator can be tuned by moving the topmost mirror by a defined distance Δz. Figure 3(d) shows experimental transmission data of a coupled microresonator with a 38 nm thick central mirror. Here, the resonance of the upper microresonator ω_1 is tuned across the fixed resonance ω_2 of the lower one and an anticrossing behavior can be observed when ω_1 is close to ω_2 and the Rabi splitting of this coupled resonator system is $\Delta\Omega = 7.9$ nm (31.9 meV). Note, that a lower and higher order mode can be seen in the experimental spectra for low and high Δz values, these modes have not been considered in the simulations. We can model such a microresonator with two coupled harmonic oscillators following Eq. (2), where the upper resonator is described by $x_1(t)$ with a tunable frequency ω_1 and the lower resonator is described by $x_2(t)$ with a fixed frequency ω_2. The respective simulations for $x_1(t)$ and $x_2(t)$ are shown in Figs. 3(e) and 3(f), respectively. From the fit of the theoretical model to the experimental data we obtain damping and coupling constants of $\gamma_1 = 11$ meV, $\gamma_2 = 50$ meV and $\kappa = 175$ meV. Again, the response of x_2 perfectly matches the experimental data, because we excite the coupled resonator from top and collect the transmission signal from below and only light from the lower resonator can reach the detector. We can separate the excitation of the lower resonator into direct excitation

Optics EXPRESS

and excitation via coupling to the upper resonator. A direct excitation is caused by leakage of the white light through the upper resonator structure due to the finite reflectivity of the upper two mirrors. However, this portion is in the range of a few percent (depending on the actual mirror thicknesses) of the incoming white light intensity since it is reflected by the two topmost mirrors. Furthermore, most wavelengths of the white light spectrum do not reach the lower resonator since they do not fulfill the resonance condition of the upper resonator. Therefore, in contrast to the single microresonator, we did not consider the spectral profile of the white light LED to reproduce the experimental data because the white light spectrum is prefiltered by the upper resonator. This creates the situation that there is only a weak direct excitation of the lower resonator, which can be considered in the simulation by modifying the starting conditions for the two oscillators. We set $x_1(0) = 1$ for the first oscillator, since it is directly excited by the white light LED, and the weak direct excitation of x_2 is taken into account by setting $x_2(0) = 0.05$. This small change of the starting conditions results in an intensity difference between the two coupled resonator modes, which is also observed in the experimental data. The second excitation pathway is the coherent energy exchange between the upper and lower resonator due to strong coupling, resulting in the observed anticrossing behavior of the two resonator modes. We find an excellent agreement between the experimental and the simulated data for these starting parameters leading to the conclusion that the lower resonator is mainly excited by coupling to the upper resonator and that the energy is coherently exchanged between the two resonators. In Fig. 3(g) experimental data is shown where the thickness of the central mirror is reduced from 38 nm to 24 nm, which increases the coupling between the two resonators modes and consequently the Rabi splitting increases from 7.9 nm (31.9 meV) to 25.7 nm (99.6 meV). The corresponding simulations for x_1 and x_2 are shown in Figs. 3(h) and 3(i) and the parameters used for the simulations are $\gamma_1 = 13$ meV, $\gamma_2 = 65$ meV and $\kappa = 360$ meV, showing that the reduction of the central mirror thickness leads to an increase of the coupling constant from $\kappa = 175$ meV to $\kappa = 360$ meV. Again, we find the best match between the response of x_2 and the experimental data. In this case the central mirror is thinner and the portion of direct excitation of x_2 is larger ($x_1(0) = 1,\ x_2(0) = 0.1$), which results in a stronger intensity difference between the two coupled modes. This effect is even more pronounced when the central mirror thickness is further reduced to 14 nm, which is experimentally shown in Fig. 3(j) and the respective simulations are presented in Figs. 3(k) and 3(l). The coupling strength between the two resonators is even larger and the Rabi splitting increases to 33.3 nm (146.1 meV). The parameters used in the simulation are $\gamma_1 = 13$ meV, $\gamma_2 = 55$ meV and $\kappa = 650$ meV and again we find the best match between x_2 and the experimental data. These results show that we have created coupled microresonators where the coupling constant can be tuned by a large amount from 175 meV to 650 meV making them ideal to study the fundamental principles of strong coupling. Interestingly, a classical damped harmonic oscillator approach is sufficient to model such strongly coupled microresonator structures and extract important parameters, i.e. the damping and coupling constants.

In summary, we prepared coupled $\lambda/2$ optical resonators which show strong coupling between the respective optical modes. The coupling strength can be adjusted by varying the thickness of the central silver mirror. Furthermore, we have shown that we can use coupled damped harmonic oscillators to theoretically describe such a strongly coupled system. For stationary conditions the white light transmission signal can be modelled by the Fourier transform of the time domain signal of the second microresonator, which is strongly coupled to the first resonator. Such a system can be used to manipulate the mode structure in the fixed microresonator without changing its geometry but by tuning the upper resonator. This may lead to exciting new applications with tunable subwavelength structures in the rapidly growing field of nanoswitches and optoelectronics. Additionally, such coupled microresonators could be used to couple molecules or other quantum systems in different compartments or over large spatial distances, i.e. placing the quantum systems in different resonators and mediate the interaction by the strongly coupled resonators.

Optics EXPRESS

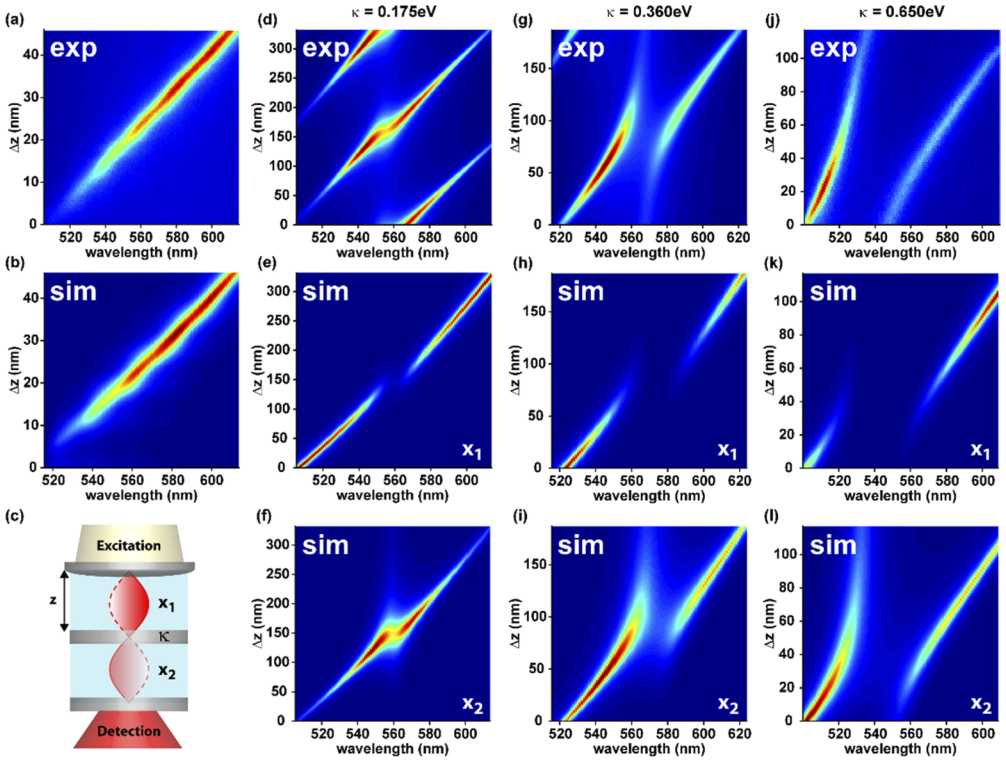

Fig. 3. (a) Experimental transmission spectra for an uncoupled microresonator where the transmission maximum is tuned by moving the upper mirror. (b) Corresponding simulations for a single microresonator. (c) Schematic drawing of the coupled microresonator, where x_1 and x_2 describe the two resonator modes. (d) Transmission spectra for a coupled microresonator and the respective simulations for x_1 and x_2 are shown in (e) and (f). The central mirror has a thickness of 38 nm resulting in a coupling constant $\kappa = 0.175$ eV and an anticrossing dispersion can be observed. (g) and (i) Experimental and simulated results for a thickness of the central mirror of 24 nm and the Rabi splitting is increased compared to (d) and (f). (j)-(l) The thickness of the central mirror is even further decreased to 14 nm leading to a larger Rabi splitting.

Another potential application might be in the rapidly emerging field of polaritonic chemistry, where interesting effects might be observed when one resonator is tuned to an electronic transition, while the other resonator is resonant to a vibration.

Funding

Ministerium für Wissenschaft, Forschung und Kunst Baden-Württemberg (Kooperatives Promotionskolleg IPMB); Deutsche Forschungsgemeinschaft (ME 1600/13-3).

Acknowledgments

The authors thank Michael Metzger and Alexander Konrad for their contribution in the initial phase of this project. We acknowledge support by Open Access Publishing Fund of University of Tübingen.

Optics EXPRESS

Disclosures

The authors declare no conflicts of interest.

References

1. E. M. Purcell, "Spontaneous Emission Probabilities at Radio Frequencies," Phys. Rev. **69**(1-2), 37–38 (1946).
2. A. Chizhik, F. Schleifenbaum, R. Gutbrod, A. Chizhik, D. Khoptyar, A. J. Meixner, and J. Enderlein, "Tuning the Fluorescence Emission Spectra of a Single Molecule with a Variable Optical Subwavelength Metal Microcavity," Phys. Rev. Lett. **102**(7), 073002 (2009).
3. M. Steiner, F. Schleifenbaum, C. Stupperich, A. Virgilio Failla, A. Hartschuh, and A. J. Meixner, "Microcavity-Controlled Single-Molecule Fluorescence," ChemPhysChem **6**(10), 2190–2196 (2005).
4. A. I. Chizhik, A. M. Chizhik, A. M. Kern, T. Schmidt, K. Potrick, F. Huisken, and A. J. Meixner, "Measurement of Vibrational Modes in Single SiO_2 Nanoparticles Using a Tunable Metal Resonator with Optical Subwavelength Dimensions," Phys. Rev. Lett. **109**(22), 223902 (2012).
5. F. Schleifenbaum, A. M. Kern, A. Konrad, and A. J. Meixner, "Dynamic control of Förster energy transfer in a photonic environment," Phys. Chem. Chem. Phys. **16**(25), 12812–12817 (2014).
6. A. Konrad, A.-L. Trost, S. Skandary, M. Hussels, A. J. Meixner, N. V. Karapetyan, and M. Brecht, "Manipulating the excitation transfer in Photosystem I using a Fabry-Perot metal resonator with optical subwavelength dimensions," Phys. Chem. Chem. Phys. **16**(13), 6175–6181 (2014).
7. J. J. Hopfield, "Theory of the Contribution of Excitons to the Complex Dielectric Constant of Crystals," Phys. Rev. **112**(5), 1555–1567 (1958).
8. P. Berman, ed., *Cavity Quantum Electrodynamics* (Academic, 1994).
9. D. S. Dovzhenko, S. V. Ryabchuk, Y. P. Rakovich, and I. R. Nabiev, "Light-matter interaction in the strong coupling regime: Configurations, conditions, and applications," Nanoscale **10**(8), 3589–3605 (2018).
10. G. Rempe, H. Walther, and N. Klein, "Observation of quantum collapse and revival in a one-atom maser," Phys. Rev. Lett. **58**(4), 353–356 (1987).
11. P. A. Hobson, W. L. Barnes, D. G. Lidzey, G. A. Gehring, D. M. Whittaker, M. S. Skolnick, and S. Walker, "Strong exciton–photon coupling in a low-Q all-metal mirror microcavity," Appl. Phys. Lett. **81**(19), 3519–3521 (2002).
12. D. Wang, H. Kelkar, D. Martin-Cano, D. Rattenbacher, A. Shkarin, T. Utikal, S. Götzinger, and V. Sandoghdar, "Turning a molecule into a coherent two-level quantum system," Nat. Phys. **15**(5), 483–489 (2019).
13. D. Wang, H. Kelkar, D. Martin-Cano, T. Utikal, S. Götzinger, and V. Sandoghdar, "Coherent Coupling of a Single Molecule to a Scanning Fabry-Perot Microcavity," Phys. Rev. X **7**(2), 021014 (2017).
14. D. Dovzhenko, K. Mochalov, I. Vaskan, I. Kryukova, Y. Rakovich, and I. Nabiev, "Polariton-assisted splitting of broadband emission spectra of strongly coupled organic dye excitons in tunable optical microcavity," Opt. Express **27**(4), 4077 (2019).
15. L. C. Flatten, Z. He, D. M. Coles, A. A. P. Trichet, A. W. Powell, R. A. Taylor, J. H. Warner, and J. M. Smith, "Room-Temperature exciton-polaritons with two-dimensional WS2," Sci. Rep. **6**(1), 33134 (2016).
16. S. Johnson, P. R. Dolan, T. Grange, A. A. P. Trichet, G. Hornecker, Y. C. Chen, L. Weng, G. M. Hughes, A. A. R. Watt, A. Auffèves, and J. M. Smith, "Tunable cavity coupling of the zero phonon line of a nitrogen-vacancy defect in diamond," New J. Phys. **17**(12), 122003 (2015).
17. J. D. Thompson, B. M. Zwickl, A. M. Jayich, F. Marquardt, S. M. Girvin, and J. G. E. Harris, "Strong dispersive coupling of a high-finesse cavity to a micromechanical membrane," Nature **452**(7183), 72–75 (2008).
18. D. G. Lidzey, D. D. C. Bradley, T. Virgili, A. Armitage, M. S. Skolnick, and S. Walker, "Room temperature polariton emission from strongly coupled organic semiconductor microcavities," Phys. Rev. Lett. **82**(16), 3316–3319 (1999).
19. T. Yoshle, A. Scherer, J. Hendrickson, G. Khitrova, H. M. Gibbs, G. Rupper, C. Ell, O. B. Shchekin, and D. G. Deppe, "Vacuum Rabi splitting with a single quantum dot in a photonic crystal nanocavity," Nature **432**(7014), 200–203 (2004).
20. D. Pellegrino, F. Pagliano, A. Genco, M. Petruzzella, F. W. Van Otten, and A. Fiore, "Deterministic control of radiative processes by shaping the mode field," Appl. Phys. Lett. **112**(16), 161110 (2018).
21. J. P. Reithmaier, G. Sek, A. Löffler, C. Hofmann, S. Kuhn, S. Reitzenstein, L. V Keldysh, V. D. Kulakovskii, T. L. Reinecke, and A. Forchel, "Strong coupling in a single quantum dot-semiconductor microcavity system," Nature **432**(7014), 197–200 (2004).
22. E. Janitz, M. Ruf, M. Dimock, A. Bourassa, J. Sankey, and L. Childress, "Fabry-Perot microcavity for diamond-based photonics," Phys. Rev. A: At., Mol., Opt. Phys. **92**(4), 043844 (2015).
23. E. Peter, P. Senellart, D. Martrou, A. Lemaître, J. Hours, J. M. Gérard, and J. Bloch, "Exciton-photon strong-coupling regime for a single quantum dot embedded in a microcavity," Phys. Rev. Lett. **95**(6), 067401 (2005).
24. E. Orgiu, J. George, J. A. Hutchison, E. Devaux, J. F. Dayen, B. Doudin, F. Stellacci, C. Genet, J. Schachenmayer, C. Genes, G. Pupillo, P. Samorì, and T. W. Ebbesen, "Conductivity in organic semiconductors hybridized with the vacuum field," Nat. Mater. **14**(11), 1123–1129 (2015).
25. P. Törmä and W. L. Barnes, "Strong coupling between surface plasmon polaritons and emitters: a review," Rep. Prog. Phys. **78**(1), 013901 (2015).
26. A. Bisht, J. Cuadra, M. Wersäll, A. Canales, T. J. Antosiewicz, and T. Shegai, "Collective Strong Light-Matter Coupling in Hierarchical Microcavity-Plasmon-Exciton Systems," Nano Lett. **19**(1), 189–196 (2019).

Optics EXPRESS

27. M. Pelton, S. D. Storm, and H. Leng, "Strong coupling of emitters to single plasmonic nanoparticles: exciton-induced transparency and Rabi splitting," Nanoscale **11**(31), 14540–14552 (2019).
28. R. Chikkaraddy, B. de Nijs, F. Benz, S. J. Barrow, O. A. Scherman, E. Rosta, A. Demetriadou, P. Fox, O. Hess, and J. J. Baumberg, "Single-molecule strong coupling at room temperature in plasmonic nanocavities," Nature **535**(7610), 127–130 (2016).
29. P. Vasa and C. Lienau, "Strong Light–Matter Interaction in Quantum Emitter/Metal Hybrid Nanostructures," ACS Photonics **5**(1), 2–23 (2018).
30. A. Konrad, A. M. Kern, M. Brecht, and A. J. Meixner, "Strong and Coherent Coupling of a Plasmonic Nanoparticle to a Subwavelength Fabry-Pérot Resonator," Nano Lett. **15**(7), 4423–4428 (2015).
31. A. Thomas, J. George, A. Shalabney, M. Dryzhakov, S. J. Varma, J. Moran, T. Chervy, X. Zhong, E. Devaux, C. Genet, J. A. Hutchison, and T. W. Ebbesen, "Ground-State Chemical Reactivity under Vibrational Coupling to the Vacuum Electromagnetic Field," Angew. Chem., Int. Ed. **55**(38), 11462–11466 (2016).
32. J. Lather, P. Bhatt, A. Thomas, T. W. Ebbesen, and J. George, "Cavity Catalysis by Cooperative Vibrational Strong Coupling of Reactant and Solvent Molecules," Angew. Chem., Int. Ed. **58**(31), 10635–10638 (2019).
33. A. Thomas, L. Lethuillier-Karl, K. Nagarajan, R. M. A. Vergauwe, J. George, T. Chervy, A. Shalabney, E. Devaux, C. Genet, J. Moran, and T. W. Ebbesen, "Tilting a ground-state reactivity landscape by vibrational strong coupling," Science **363**(6427), 615–619 (2019).
34. E. Kapon, J. Katz, and A. Yariv, "Supermode analysis of phase-locked arrays of semiconductor lasers," Opt. Lett. **9**(4), 125–127 (1984).
35. C. Xia, N. Bai, I. Ozdur, X. Zhou, and G. Li, "Supermodes for optical transmission," Opt. Express **19**(17), 16653 (2011).
36. J. Zhou, "Analytical formulation of super-modes inside multi-core fibers with circularly distributed cores," Opt. Express **22**(1), 673 (2014).
37. C. Guan, L. Yuan, and J. Shi, "Supermode analysis of multicore photonic crystal fibers," Opt. Commun. **283**(13), 2686–2689 (2010).
38. L. Michaille, C. R. Bennett, D. M. Taylor, T. J. Shepherd, J. Broeng, H. R. Simonsen, and A. Petersson, "Phase locking and supermode selection in multicore photonic crystal fiber lasers with a large doped area," Opt. Lett. **30**(13), 1668 (2005).
39. M. Bayer, T. Gutbrod, J. P. Reithmaier, A. Forchel, T. L. Reinecke, P. A. Knipp, A. A. Dremin, and V. D. Kulakovskii, "Optical modes in photonic molecules," Phys. Rev. Lett. **81**(12), 2582–2585 (1998).
40. M. Zhang, C. Wang, Y. Hu, A. Shams-Ansari, T. Ren, S. Fan, and M. Lončar, "Electronically programmable photonic molecule," Nat. Photonics **13**(1), 36–40 (2019).
41. M. Galbiati, L. Ferrier, D. D. Solnyshkov, D. Tanese, E. Wertz, A. Amo, M. Abbarchi, P. Senellart, I. Sagnes, A. Lemaître, E. Galopin, G. Malpuech, and J. Bloch, "Polariton condensation in photonic molecules," Phys. Rev. Lett. **108**(12), 126403 (2012).
42. J. Wang, Y. Yin, Q. Hao, Y. Zhang, L. Ma, and O. G. Schmidt, "Strong Coupling in a Photonic Molecule Formed by Trapping a Microsphere in a Microtube Cavity," Adv. Opt. Mater. **6**(1), 1700842 (2018).
43. Y. P. Rakovich and J. F. Donegan, "Photonic atoms and molecules," Laser Photonics Rev. **4**(2), 179–191 (2009).
44. K. A. Atlasov, A. Rudra, B. Dwir, and E. Kapon, "Large mode splitting and lasing in optimally coupled photonic-crystal microcavities," Opt. Express **19**(3), 2619 (2011).
45. T. Cai, R. Bose, G. S. Solomon, and E. Waks, "Controlled coupling of photonic crystal cavities using photochromic tuning," Appl. Phys. Lett. **102**(14), 141118 (2013).
46. A. R. A. Chalcraft, S. Lam, B. D. Jones, D. Szymanski, R. Oulton, A. C. T. Thijssen, M. S. Skolnick, D. M. Whittaker, T. F. Krauss, and A. M. Fox, "Mode structure of coupled L3 photonic crystal cavities," Opt. Express **19**(6), 5670 (2011).
47. K. A. Atlasov, K. F. Karlsson, A. Rudra, B. Dwir, and E. Kapon, "Wavelength and loss splitting in directly coupled photonic-crystal defect microcavities," Opt. Express **16**(20), 16255–16264 (2008).
48. A. Konrad, M. Metzger, A. M. Kern, M. Brecht, and A. J. Meixner, "Controlling the dynamics of Förster resonance energy transfer inside a tunable sub-wavelength Fabry-Pérot-resonator," Nanoscale **7**(22), 10204–10209 (2015).
49. M. Steiner, A. V. Failla, A. Hartschuh, F. Schleifenbaum, C. Stupperich, and A. J. Meixner, "Controlling molecular broadband-emission by optical confinement," New J. Phys. **10**(12), 123017 (2008).
50. P. B. Johnson and R. W. Christy, "Optical Constants of the Noble Metals," Phys. Rev. B **6**(12), 4370–4379 (1972).